Lab on a Secchi disk: A prototype open-source profiling package for low-cost monitoring in aquatic environments

Robert J. W. Brewin [1,2]* Thomas G. Brewin,[2,3] Philip J. Bresnahan [4] Keiley Davis,[1] Xuerong Sun,[1] Nicola Wilson,[1] Lars Brunner,[5] Giorgio Dall'Olmo[6]

[1]Centre for Geography and Environmental Science, Department of Earth and Environmental Sciences, University of Exeter, Cornwall, UK
[2]Brewtek Ltd, Kent, UK
[3]Chatham and Clarendon Grammar School, Kent, UK
[4]Department of Earth and Ocean Sciences, University of North Carolina Wilmington, Wilmington, North Carolina, USA
[5]Scottish Association for Marine Science, Scottish Marine Institute, Oban, Scotland, UK
[6]National Institute of Oceanography and Applied Geophysics – OGS, Trieste, Italy

Abstract

Owing to the high cost of commercial optical sensors, there is a need to develop low-cost optical sensing packages to expand monitoring of aquatic environments, particularly in under-resourced regions. Visual methods to monitor the optical properties of water, like the Secchi disk and Forel-Ule color scale, remain in use in the modern era owing to their simplicity, low-cost and long history of use. Yet, recent years have seen advances in low-cost, electronic-based optical sensing. Here, the designs of a miniaturized hand-held device (mini-Secchi disk) that measures the Secchi depth and Forel-Ule color are updated. We then extend the device by integrating a small electronic sensing package (Arduino-based) into the Secchi disk, for vertical profiling, combining historic and modern methods for monitoring the optical properties of water into a single, low-cost sensing device, that measures positioning (GPS), light spectra, temperature, and pressure. It is charged and transfers data wirelessly, is encased in epoxy resin, and can be used to derive vertical profiles of spectral light attenuation and temperature, in addition to Secchi depth and Forel-Ule color. We present data from a series of deployments of the package, compare its performance with commercially available instruments, and demonstrate its use for validation of satellite remotely sensed data. Our designs are made openly available to promote community-based development and have potential in communicating and teaching science, participatory science, and low-cost monitoring of aquatic environments.

Aquatic systems are under increasing anthropogenic pressure (Pinsky and Fredston 2022). To manage these pressures and mitigate impacts to society, monitoring systems are needed capable of collecting data on environmental indicators at appropriate temporal and spatial scales (von Schuckmann et al. 2021). Important environmental indicators to monitor include the optical properties of natural waters. They are useful for tracking the health and functioning of aquatic

ecosystems, and tracking the concentrations of water constituents present, such as sediments, pollutants, organic matter, and phytoplankton (IOCCG 2000).

While high-tech monitoring (e.g., satellite visible radiometry and ocean robotic platforms; Groom et al. 2019; Chai et al. 2020) has revolutionized our ability to monitor the aquatic realm optically, data collection in situ remains at the heart of aquatic optics, connecting and ground truthing other measurements and expanding our understanding of the subject. Yet, owing to the challenging nature of aquatic environments, commercial in situ optical equipment is often expensive, and consequently not widely accessible. Furthermore, the size and cost of the equipment means it is often not suitable for deployment in hard-to-access regions. For audiences with limited financial resources, there is a clear need for affordable optical sensing packages, that can be deployed in a wide range of environments and from a variety of platforms, to help democratize and expand in situ optical monitoring of aquatic waters.

*Correspondence: r.brewin@exeter.ac.uk

Robert J. W. Brewin and Thomas G. Brewin contributed equally to this study.

This need has spurred the development of low-cost, small, and efficient electronic optical sensing packages (often Arduino or Raspberry Pi based) for in situ aquatic monitoring (Butler and Pagniello 2021). Sometimes documented in "do-it-yourself" (DIY) projects, and using open-source tools, these developments promote a more inclusive and participative approach to aquatic monitoring, and they can be more accessible to those who struggle to afford commercial equipment. Sometimes benefiting from use in connection with mobile phones (e.g., wireless data transfer or use of mobile phone cameras as sensors), examples of low-cost optical sensing packages include those that focus on diffuse attenuation (Bardaji et al. 2016; Rodero et al. 2022), fluorometry (Leeuw et al. 2013; Friedrichs et al. 2017; Hixson and Ward 2022), remote-sensing reflectance (Hommersom et al. 2012; Leeuw and Boss 2018; Burggraaff et al. 2019, 2022), turbidity (Parra et al. 2018; Wang et al. 2018; Gillett and Marchiori 2019; Droujko and Molnar 2022; Rocher et al. 2023), and backscattering (Eidam et al. 2022, also https://iorodeo.com/). The miniaturization and adaptability of the technology also means there is potential to deploy such packages on a wider variety of platforms, from to marine vertebrates to watersports equipment (Brewin et al. 2017; Harcourt et al. 2019; Griffiths et al. 2021; Bresnahan et al. 2022), expanding the range of environments amenable to in situ data collection.

Another solution for more affordable optical monitoring is to modernize traditional visual-based in situ techniques. The Forel-Ule color scale (Forel 1890; Ule 1892), consisting of 21 colors ranging from blue to green to yellow to brown (Wernand and van der Woerd 2010), has seen a resurrection in use (Ye and Sun 2022), with the development of a more modern version (Novoa et al. 2014) and integration into mobile phone applications (Novoa et al. 2015; Busch et al. 2016; Malthus et al. 2020). The Secchi disk (Secchi 1864), a (typically) white disk that is lowered into the water with the depth at which it disappears (Secchi depth) being proportional to the clarity or transparency of the water (Wernand 2010), is still being used routinely today (Lee et al. 2018*a*), benefitting from data logging though mobile phone applications (e.g., Seafarers et al. 2017; Kirby et al. 2021). Brewin et al. (2019) recently developed a hand-held, partly 3D-printed, device (mini-Secchi disk) for measuring the Secchi depth and Forel-Ule color of lake, estuarine and nearshore regions, that was designed for ease of use in smaller water bodies, and from small watercraft and platforms. With over 400 mini-Secchi disks built to date, the devices have proven useful in participatory science projects (George et al. 2021), for evaluating satellite observations (Kulk et al. 2021), and for empowering citizen monitoring of local water bodies (Menon et al. 2021).

Both approaches to affordable optical sensing, low-cost electronic packages and modernizing traditional visual-based techniques, have advantages and disadvantages. For example, low-cost electronic optical sensing packages can directly measure key apparent optical properties without biases caused by variations in vision among participants (e.g., *see* Burggraaff et al. 2021). On the other hand, visual-based techniques like the Secchi depth and Forel-Ule measurements are less prone to failure (e.g., from electronic components failing), build on a long tradition in optical limnology and oceanography, meaning they have been rigorously tested over the years with long-time-series data available in some regions (Boyce et al. 2010; Wernand et al. 2013; Kahru et al. 2023), and are useful for teaching the basic concepts (and history behind) optical limnology and oceanography.

Rudolph W. Preisendorfer, one of the leading experts on interpreting Secchi depth readings, and with reference to deriving inherent and apparent optical properties from the Secchi depth, warned against over-usages of its application in what he deemed as "Secchi disker madness." Specifically, in his 1986 NOAA technical memorandum, he states (under the subsection Secchi disker madness) "But if I am going to go so far as to build or rent or buy these instruments [referring in the previous sentence to a transmissometer and an irradiance meter], dip them in, and then reduce the data, then … I will really not need the Secchi disk, except perhaps for sentimental reasons" (Preisendorfer 1986, p. 39). A point also made in an earlier paper by Tyler (1968). Here, we begin by updating the designs of the mini-Secchi disk, through user feedback. Next, and while fully aware of Preisendorfer's statement on "Secchi disker madness," we integrate a small electronic sensing package (Arduino-based) into the Secchi disk, to collect vertical profiles of spectral irradiance and temperature. We describe how the device is constructed and operated, compare its performance with commercially available instruments, and demonstrate its use for the evaluation of remotely sensed ocean color data. All designs are made openly available to promote further community-based development, and we discuss the benefits of the device, while providing a justification as to why we think we have not gone mad.

Materials and procedures

Updates to the design of the mini-Secchi disk

The original mini-Secchi disk design (Brewin et al. 2019), available openly in their publication, received extensive use in two participatory (citizen) science projects: the Rehabilitation of Vibrio-infested waters of Lake Vembanad (REVIVAL) project funded under the India–UK Water Quality programme (https://www.pml.ac.uk/science/projects/REVIVAL), which involved citizen sampling of Lake Vembanad the largest body of water in Kerala, India (George et al. 2021); and the Multiscale Observation Networks for Optical monitoring of Coastal waters, Lakes and Estuaries (MONOCLE) project, funded by the European Union (https://www.monocle-h2020.eu), which involved citizen sampling in a number of lakes in Europe and Africa. With around 200 of the original mini-Secchi disk designs produced for these projects, we actively encouraged feedback from users (through face-to-face discussions and email), which

fed into improvements in the design outlined in detail in Supplementary Table S1.

In general, the key modifications to the new designs include: the body of the device being redesigned to hold more tape and minimize friction during operation; the production of a 2nd larger (but still hand-held) device (named a midi-Secchi disk) that holds a 20 m tape, for measurements in coastal waters (*see* Supplementary Fig. S1); certain components (handle, lanyard and finger strap) strengthened to minimize cases of failure; a pH paper attachment added; and a switch from polylactic acid (PLA) to tough PLA (TPLA) to enhance the strength and durability of the device. The device is still manufactured in the same way, using primarily a 3D printer and basic workshop tools. We have switched to using an Ultimaker S5 (rather than 2 and 2+) with open-source 3D printing software Ultimaker Cura for recent prints, though the device can be manufactured using most 3D printers and associated software (including the Ultimaker 2 and 2+). The new stereolithography files (STL) for all 3D-printed parts (and the weight) are openly available (*see* https://github.com/rjbrewin/Sensing-Secchi-Disk). Further details on the construction of the device can be found in Brewin et al. (2019).

We recently made 100 of the new devices for a citizen/community science effort as part of the Sustained Ocean Color Observations with Nanosatellites (SOCON) project (Bresnahan et al. 2023), where we hope to elicit further feedback and future improvement to these new designs. Mobile phone apps are available for data logging, that were successfully developed in the REVIVAL (George et al. 2021) and MONOCLE (https://www.monocle-h2020.eu/Sensors_and_platforms/Mini-secchi_disk_en) projects. The new version of the device has found use in communicating and teaching some of the basic concepts and history behind optical limnology and oceanography, through undergraduate classes and outreach events (*see* Supplementary Fig. S1).

The sensing Secchi disk prototype

The sensing Secchi disk (SSD) was introduced as a simple replacement of the Secchi disk on the mini-Secchi or midi-Secchi. Designed to still operate as a Secchi disk, we integrated a sensor package within the disk to measure positioning (GPS), spectral light, temperature, and pressure, and that can be charged, and transfer data, wirelessly. The device is entirely encased in epoxy resin. Details of all the components used in the prototype we developed are listed in Supplementary Table S2.

The initial prototype of the disk (Fig. 1) is 30 mm thick and 100 mm in diameter (same diameter as the mini-Secchi disk). The diameter of the disk is considered suitable for measuring Secchi depths up to around 20 m, with the angular subtense of the disk's radius (radius/Secchi depth) being the same as standard ocean disk of 300 mm at a Secchi depth of 60 m. The diameter could be increased for ocean applications. It is contained within two 3D-printed cases, representing the top and bottom of the disk. The top case contains a 5-mm hole for fitting an optical diffuser (ground glass, 1.6 mm thick, 120 Grit, Edmund Optics) that sits above a spectral irradiance sensor (AS7341 sensor) measuring eight separate overlapping bands of colored light (centered at 415, 445, 480, 515, 555, 590, 630, and 680 nm, with full width half maximum values increasing from 26 to 52 nm from 415 to 680 nm), one band of near-infrared and an integrated/unfiltered band (clear channel) that constitutes a photodiode without a filter. After some testing in the United Kingdom, the analog-to-digital converter for the AS7341 was configured with an integration time of 100 ms, and with a gain of four, for all channels in the visible spectrum, consistent with Bäumker et al. (2021). However, these settings can be adjusted to a specific light environment. The upward facing sensor is designed specifically for measuring spectral downwelling diffuse attenuation ($K_d(\lambda)$), computed as a relative change in spectral downwelling irradiance with depth, though it could be calibrated to measure absolute irradiance (not conducted here). The relative change measurement offers significant advantages in low-cost, DIY sensors, especially in participatory science projects, in that they are calibration and stability independent. The bottom case contains two inlets, one with an exposed pressure sensor (MS5803-14BA) protected with a small cover, and the other with an exposed temperature sensor (TMP117). The device is operated using an Arduino MRK1000 (or MRK1010 as the MRK1000 has recently become discontinued) microcontroller with Wi-Fi connectivity to coordinate data logging and transfer. It is connected to a GPS sensor (Adafruit Ultimate GPS Breakout) for logging positioning and updating the clock on the microcontroller, and a flash SD Card (512 MB) for storing data. It is powered by a lithium polymer battery (850–1000 mAh) and charged using a wireless charging module (5 V/1 A or 5 V/5 A). An additional thermistor (10K Precision Epoxy) is also used as a proxy for internal temperature of the device. All components of the device cost around 309 GBP (~390 USD), with significant potential to reduce costs further, using either purpose-built printed circuit boards or similar but cheaper components. The device can be built with access to basic workshop tools and a 3D printer.

Manufacturing the SSD

A wiring diagram for the SSD is provided in Supplementary Fig. S2, which details how the device is connected, and Fig. 2 shows some of the key steps in the manufacturing process. Once components (Supplementary Table S2) were sourced, and 3D-printing completed for the two cases (top and bottom), supports for brass rod, charging paddle, magnet key, and potting shell, manufacturing commenced.

At first all components were checked and tested. This entailed connecting (using a breadboard) each sensor to the Arduino, and checking voltage, current, and data output and response. The AS7341 was then modified (removing the SparkFun Qwiic compatible Stemma QT connectors) with the
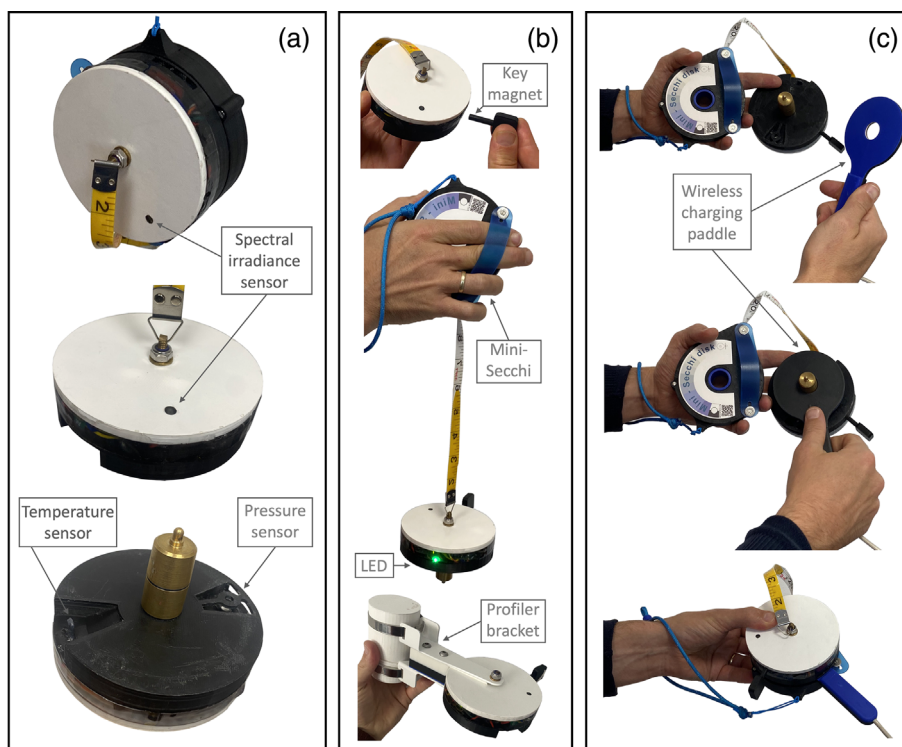
Fig. 1. (**a**) The SSD, showing the locations of the spectral irradiance, temperature, and pressure sensors. (**b**) Operating the SSD, attaching the key magnet and waiting for the green LED to indicate the device is collecting data and ready for profiling. Operating using a mini-Secchi disk or a tailor-made profiling bracket. (**c**) Charging the SSD using the wireless paddle (after adding the key magnet) and switching the device into data transfer mode.

optical diffuser very carefully placed over the light sensor and secured with a little fast curing (Gorilla Epoxy) resin (Fig. 2a). The TMP117 was coated in thermally conductive epoxy (8329TFS MG Chemicals) and the brass rod connected to a mini-Secchi disk weight using a tap and die set and a drill (Fig. 2a). We built the SSD from the bottom upwards, first by placing the wireless charging unit, pressure sensor (MS5803-14BA) and temperature sensor (TMP117) in their allocated slots on the bottom case and securing them, using a little of the fast-curing epoxy resin, being very careful not to get any resin on the gel of the MS5803-14BA sensor or the TMP117 sensor (Fig. 2b). We also built a voltage divider (for monitoring the voltage of the device), secured the internal temperature sensor (with the end placed next to the breakout board of the TMP117), added a green LED, and fastened the SD card on the bottom case (Fig. 2b). We then added the microcontroller (Arduino MRK1000/MRK1010) and the lithium battery (encased in a thin layer of foam, to cater for any expansion of the battery over time, and having added a reed switch onto the positive power cable) on top (Fig. 2b), before finally adding in the brass rod (with 3D-printed support rings), the GPS (Adafruit Ultimate GPS Breakout), securing the AS7341 to the top case, completing all wiring, adding the LED circuit, connecting the battery and wireless charger to micro-controller (the latter by connecting the Micro USB B port),

closing the unit, and securing it by screwing a nylon threaded stainless steel nut with washer onto the brass rod (Fig. 2b). At this point, prior to potting, the SSD was then checked and tested.

The SSD was then placed into its 3D-printed potting shell and sealed using packaging tape and a glue gun (Fig. 2c). Craft resin was then poured into the potting shell and left to cure over a 72-h period (Fig. 2c). Once set, the potting shell was removed and we drilled a 5-mm hole alongside (but avoiding) the reed switch, to create a space for attaching the magnet key that switches the device on and off (Fig. 2d). With the optical diffuser glass covered (using Blue-Tack), and the bottom of the device protected with tape, the top surface was sprayed in white spray paint for enhancing the reflectance of the surface (Secchi) disk. Finally, the magnet key (adding the neodymium magnets to the 3D-printed key) and wireless charging paddle were made, and the device was checked and tested (Fig. 2d). We also designed a profiling bracket (that was waterjet cut) for connecting the SSD to a profiling rig for testing it alongside commercial sensors (*see* Fig. 1b). Files (STL) for all printed parts are provided openly (*see* https://github.com/rjbrewin/Sensing-Secchi-Disk).

Operating the SSD

The SSD prototype was designed to operate in two modes, data collection mode and data transfer mode. The switch
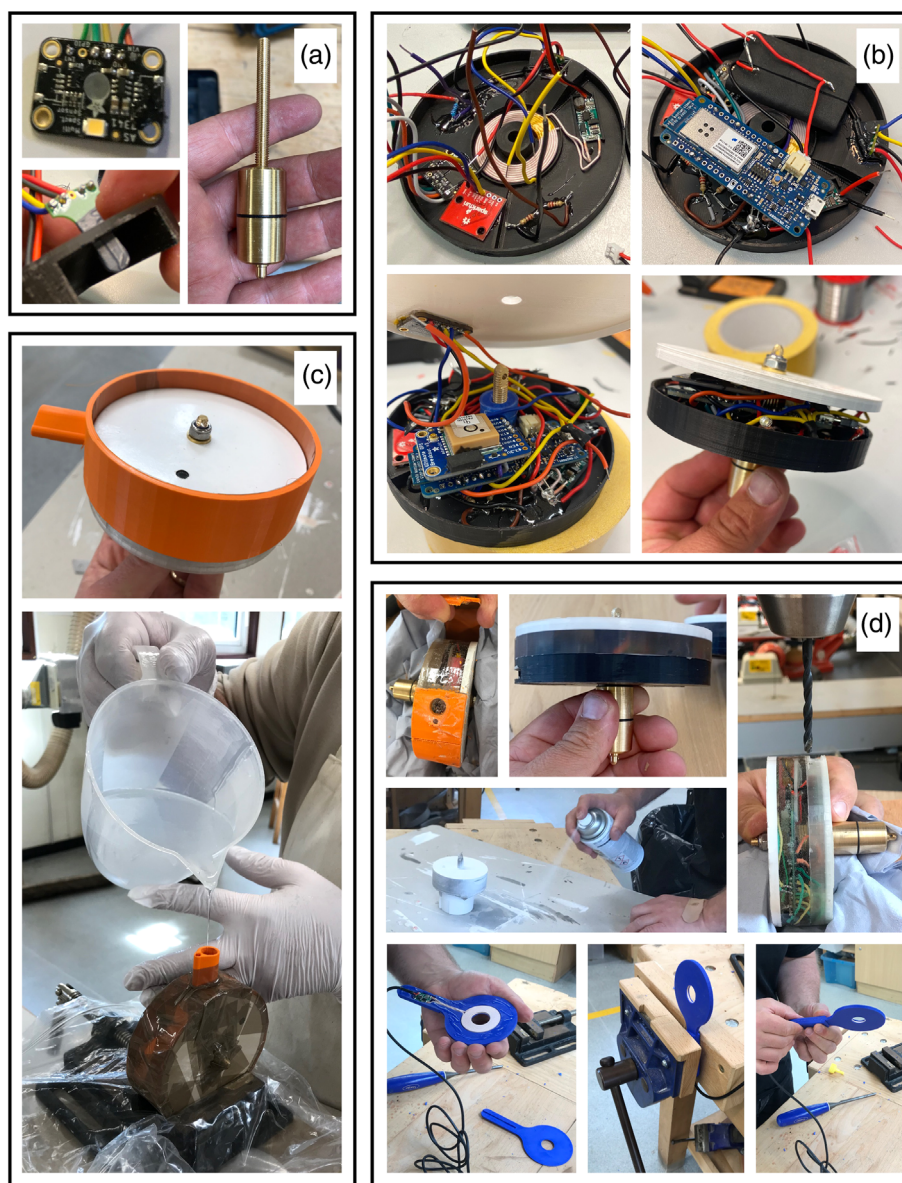
Fig. 2. Manufacturing the SSD. (**a**) Attaching diffuse glass to the spectral irradiance sensor (AS7341), coating the temperature sensor (TMP117) with thermally conductive epoxy and sinking it into the base of the device, and connecting the brass rod to the weight. (**b**) Building the device from bottom upwards, adding components and wiring. (**c**) Potting the device using the potting shell, sealing with tape and glue, and adding epoxy resin. (**d**) Removing the potting shell, drilling the magnet hole, spraying the disk, and manufacturing the wireless charger.

between the two modes was set based on the voltage. When the SSD is running directly from the battery ($\sim$3.7 V) it operates in data collection mode and when the wireless charger is connected (running at $\sim$5 V) the SSD operates in data transfer mode. The SSD is started by attaching the magnet key, which connects the circuit through the reed switch. Once running in data collection mode, the device searches for a GPS fix, logging the longitude and latitude, and updating the clock on the microcontroller. There is currently a 5-min period where, if the GPS has not found a fix, the instrument starts collecting data without a fix or an update to the clock. A green

LED switches on to indicate the device is collecting data at which point it can be used for profiling.

We recommend acclimating the device just below the surface of the water for 2 min prior to profiling, and to profile at <20 cm per second to ensure the TMP117 is responding in time with depth changes in temperature. The device was designed to profile in the top 10–20 m of the water column (in-line with the tape lengths of the mini- and midi-Secchi disk), but testing has shown it is capable of profiling repeatedly to 50 m, with one device tested to further depths, failing to record data beyond 70 m (*see* "Assessment" section). Given

the device is entirely encased in epoxy, it is envisaged minor changes in its design should allow it to profile to much deeper depths, if necessary, noting the pressure sensor is rated to ∼140 m. The device collects time-stamped data at >1 Hz, which is written to a date-stamped csv file on the SD card that also contains the co-ordinates from the GPS in the header. When multiple files are collected on the same day, they are named by adding a number sequentially after the date. Once data have been collected, the device is switched off by removing the magnet key. We recommend measuring the Secchi depth and Forel-Ule color data on a separate cast immediately after profiling, so as not to impact the speed of the profile.

To charge the battery and switch the device into data transfer mode, the wireless charger paddle (Fig. 1c) is connected to the base of the device (sits neatly around the weight and between the body of the mini-Secchi and the SSD) and the magnet key is reconnected (to allow the battery to charge). The SSD then operates as a webserver (using the Arduino WiFi101 library for the MRK1000 or WiFiNINA library MRK1010) where it allows the user to connect to the device through WiFi and communicate with it via HTML requests. Once connected to the server (initially named "Sensing_Secchi_XXX," where XXX refers to the serial number of the device) the user connects through HTML (for Arduino MKR1000, http://192.168.1.1; for the Arduino MKR1010, http://192.168.4.1). A page appears listing all the file names on the device (*see* Supplementary Fig. S3A). The user then types and submits the filename they would like to access. If they want to access the data, they can click on a link which takes them to a webpage to submit the Secchi depth, Forel Ule, and pH (if taken) readings for the profile, then click another link to get the data (*see* Supplementary Fig. S3B). The data from the file are then transferred in the following webpage (*see* Supplementary Fig. S3C) and the user can then save the data to their machine (e.g., by clicking file, save as, and saving as a ".txt" file). By moving back to the home page (Supplementary Fig. S3A), the user then has the option to delete files (required to not clog up the 512 MB SD card, *see* Supplementary Fig. S3D). There is also an option to update firmware on the device wirelessly, by uploading a new sketch (name for an Arduino program) over the network using the ArduinoOTA package (Supplementary Fig. S3E). The sketch for the SSD is written in the Arduino programming language (based on C++) and openly available (both MRK1000 and MRK1010 versions, *see* https://github.com/rjbrewin/Sensing-Secchi-Disk).

Processing SSD data

Once ".txt" files have been saved to a computer, they can be easily read using a range of software. We have provided a simple Python Jupyter Notebook (https://github.com/rjbrewin/Sensing-Secchi-Disk) that demonstrates how to read a file from a profile and plot key variables. There are a few aspects of the processing worth noting. First, we convert

pressure readings to depth, by first subtracting an estimate of atmospheric pressure. We do that by taking a median of the first five readings once the device begins to operate, which assumes it has not been lowered into the water at the point it begins operating. This method may help correct for any drift in the calibration of the pressure sensor. Second, depths are corrected to align to the spectral light sensor, which is ∼20 mm above the pressure sensor, and the temperature sensor, ∼7 mm below the pressure sensor. As discussed above, we recommend a 2-min surface acclimation of the device prior to profiling. One simple method to extract a clean downcast is to remove data prior to completion of the 2-min surface acclimation by selecting the point at which a consistent positive downward gradient in pressure is identified. The average spectral diffuse attenuation coefficients ($K_d(\lambda)$) above a specific depth can be computed by fitting a Beer–Lambert law to the light profiles above that depth (e.g., the Secchi depth or maximum depth of the profile). Additionally, profiles of spectral diffuse attenuation coefficients ($K_d(\lambda,z)$) can also be extracted by dividing the logarithmic difference between consecutive light measurements by the difference in depth.

Assessment

Trelissick pontoon, Falmouth, England

We evaluated the performance of an SSD (SSD003) at Trelissick pontoon on 03 February 2023 (Fig. 3a,b), which protrudes in the Fal Estuary, Cornwall, UK (50.216 N, 5.0277 W), for water depths from 0 to 5 m. The pontoon had been used successfully for undergraduate student teaching using the mini-Secchi disk (*see* Supplementary Fig. S1E). Thirteen deployments were conducted at 30-min intervals from around 10:00 to 16:00 GMT, encompassing a tidal cycle from low (∼10:00) to high tide (∼16:00). For each profile, we conducted deployments of the SSD003 alongside two commercial instruments, a CastAway conductivity–temperature–density (CTD) profiler and an AML Minos CTD profiler. These instruments collected temperature and salinity profiles. They were selected due to their well-documented performance and considering they encompass both relatively low-cost (CastAway, costing ∼£5000) and relatively higher-cost (AML Minos, costing > £10,000) CTD profilers. The CastAway had been previously calibrated on 01 October 2019 and the Minos on 01 February 2022.

For each of the 13 deployments, and due to handling capacity, the AML Minos was deployed first (Fig. 3c), allowing 30 s of acclimatization in the top 0.5 m of the water column before slowly lowered to the seabed, waiting 10 s then conducting the upcast. Once deployment of the AML Minos CTD had been completed, the SSD and Castaway were deployed simultaneously (Fig. 3d) using the same procedure but acclimating for around 2 min at the surface (given both temperature sensors on the CastAway and SSD do not respond as quickly as the AML Minos thermistor does). These devices
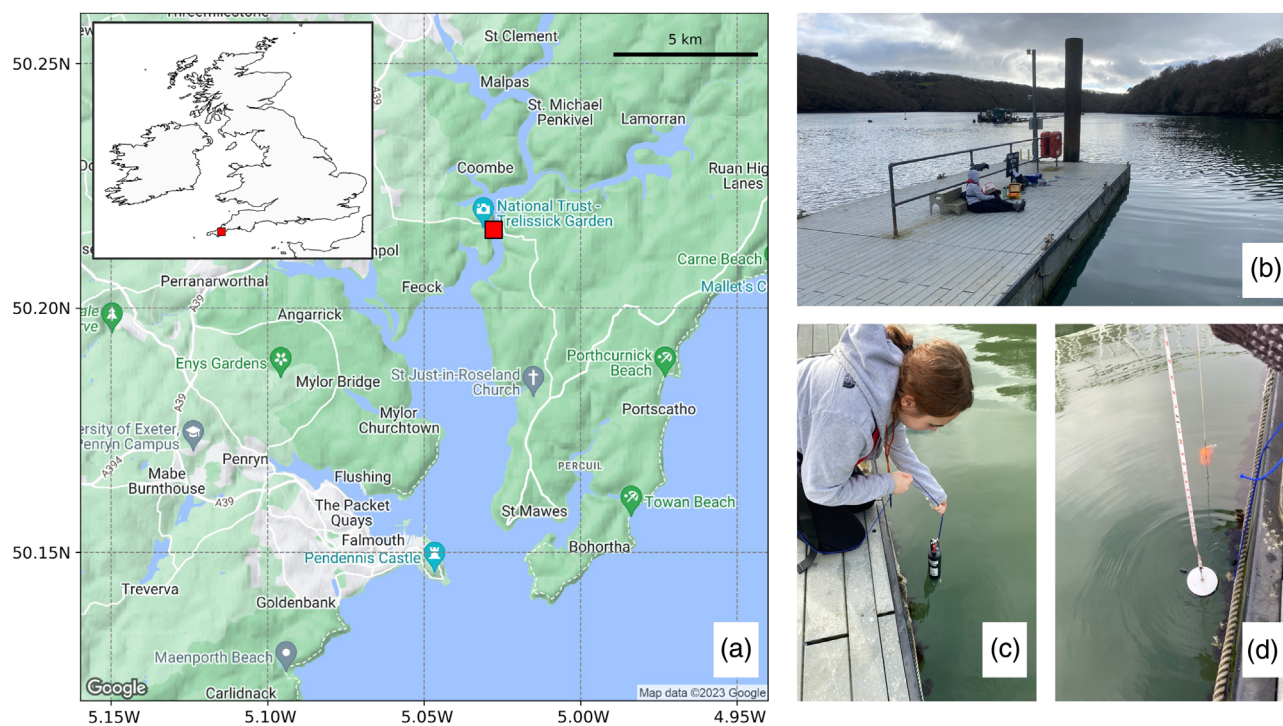
Fig. 3. (**a**) Location of Trelissick pontoon (red square) in the Fal Estuary, Cornwall, UK (background image from Google Maps). (**b**) Photograph of Trelissick pontoon during data collection on 03 February 2023. (**c**) Deployment of the AML Minos CTD. (**d**) Simultaneous deployment of the SSD and CastAway CTD.

were deployed at around 5 cm per second. Following completion of the profiles (both up and down casts), the SSD was deployed for a 2nd time to conduct Secchi depth (Z_{SD}) and Forel-Ule color measurements (color of disk at ~1/2 Secchi depth). This was repeated for each of the 13 deployments.

The SSD003 temperature profiles were processed as follows. First, we computed the cumulative sum of the gradient in the depth measurements and selected a cut off value of 0.08 (chosen from an analysis of the cumulative sums of each profile) to remove data before and after the profile commenced. For the downcast, we removed any data that did not stay above the cut off value for more than 10 measurements. The downcast and upcasts were then partitioned around the maximum depth reached. This procedure was found to remove data while the instrument was acclimating before the downcast, and when it was at the surface after completing the upcast (*see* Supplementary Fig. S4 for an example of the procedure and Supplementary Fig. S5 for extracted downcast and upcasts for all stations). In general, both downcast and upcasts were in reasonable agreement, suggesting the TMP117 sensor was responding well to temperature variations in the water, with some minor differences (within the 0.1°C accuracy of the TMP117 sensor as reported by the manufacturer) for some profiles, that may reflect real variations between the times of the downcast and upcast (*see* Supplementary Fig. S5). The SSD003 downcast was selected for the comparison with the CastAway

and AML Minos CTDs. The CastAway was programmed to collect data using processed settings (recommended by manufacturers and consisting of a weighted average of the downcast and upcast), which provided data every ~30 cm depth (starting ~15 cm below the surface). The AML Minos begins operating once submerged and collects data at >1 Hz. We extracted the downcast from each profile of the AML Minos, by selecting data prior to the point the maximum depth was reached. To quantitatively compare measurements, we extracted temperature data from the SSD003 and AML Minos at the same depths as the CastAway (which had the coarsest depth resolution) through data interpolation. We also gridded the three datasets onto a common depth axis as a function of time, for producing contour plots.

Downcast profiles for the three instruments were in reasonable agreement, but with a systematic difference for the CastAway (*see* Supplementary Fig. S6). The mean difference (δ) in temperature between the SSD003 and the AML Minos was −0.04°C with a mean absolute deviation of 0.02°C, showing the TMP117 sensor on the SSD was performing within the 0.1°C accuracy reported by the manufacturer, when taking the AML Minos CTD to be the truth (Fig. 4a). The mean difference (δ) in temperature between the CastAway and SSD003 was much higher, at 0.19°C, with a mean absolute deviation (Δ) of 0.03°C (Fig. 4b). This systematic difference in the CastAway was also seen (albeit slightly smaller at 0.14°C) when
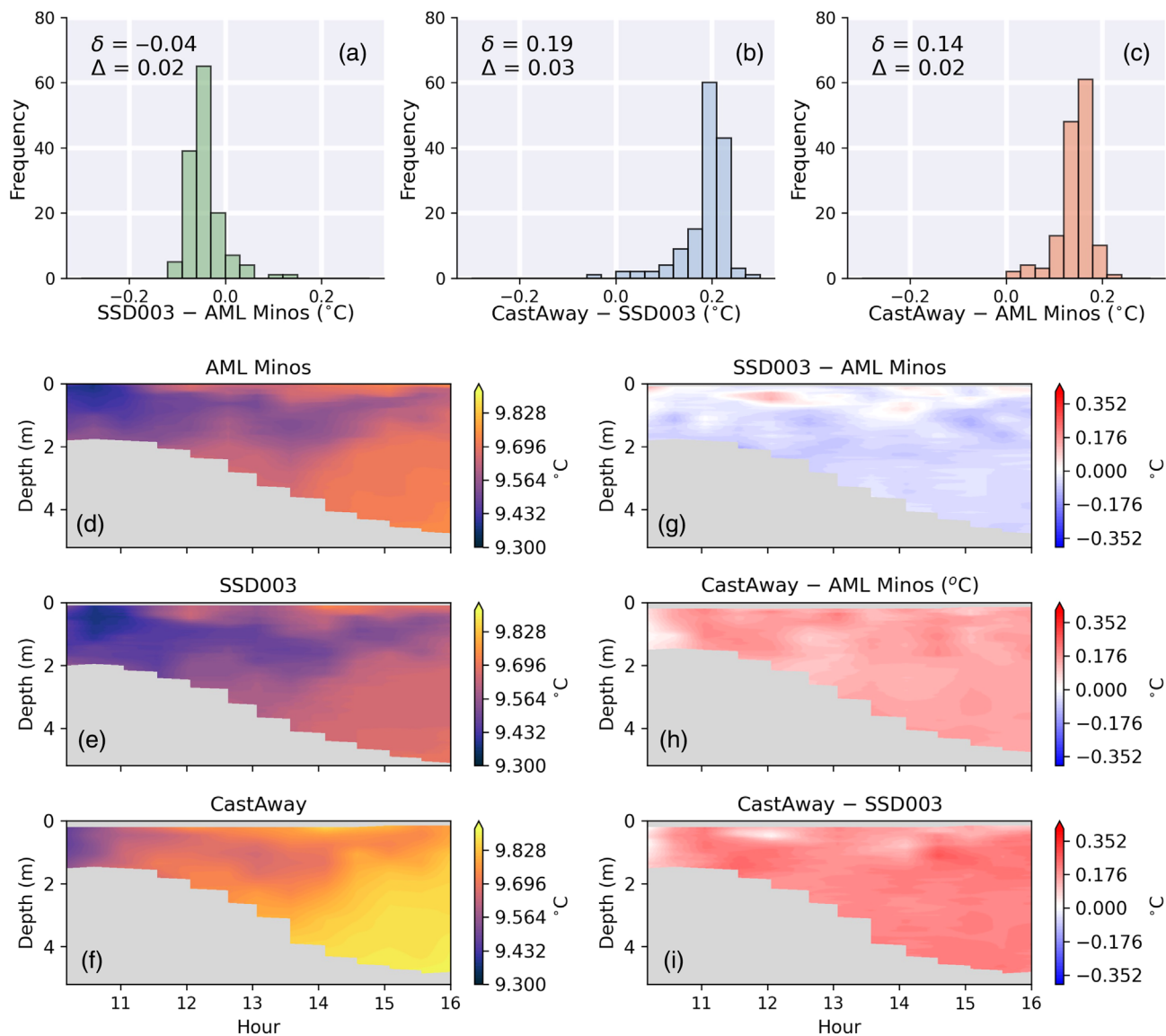
Fig. 4. Comparison of temperature profiles among the SSD003, CastAway, and AML Minos instruments, collected over a tidal cycle at Trelissick pontoon on 03 February 2023. (**a**) Histogram of differences between the SSD003 and AML Minos, (**b**) CastAway and SSD003, and (**c**) CastAway and AML Minos. δ is the mean difference and Δ the mean absolute deviation. (**d–f**) Contour plots of the temperature profiles from the three instruments over the tidal cycle. (**g–i**) Contour plots of the differences in temperature from the three instruments over the tidal cycle.

compared with the AML Minos (Fig. 4c). It is worth noting that the CastAway had not been calibrated since October 2019, and that this difference may simply reflect a drift in the sensor since the last calibration. The mean absolute deviation between CastAway and AML Minos (0.02°C) was the same as between the SSD003 and AML Minos (Fig. 4a,c). Contour plots show strong similarities among instruments in the features of temperature profiles over the tidal cycle, with denser (saltier) but warmer seawater at depth, pushing up as the tide rises, and less dense (fresher) but cooler freshwater sitting closer to the surface, with a layer at the very surface heating over the course of the day (Fig. 4d–f). Contour plots

of the differences between sensors (Fig. 4g,i) generally reflect the mean differences (bias) shown in the histograms (Fig. 4a–c), but the biases between SSD003 and AML Minos do show depth variation, being slightly positive near the surface and negative at depth. Overall, the comparison indicates the SSD003 performs well at collecting temperature profiles in the upper 5 m, comparable in performance to the CastAway when tested against a high-grade CTD (AML Minos).

Light profiles collected at Trelissick pontoon were processed in the same way as the temperature profiles, with the only difference being that we removed data for each profile (both down and upcast) 10 cm from the maximum depth, to

remove erroneous data caused by the sensor disturbing the seabed (Supplementary Fig. S7). The 3rd of February 2023 was an overcast day at Trelissick pontoon (*see* Fig. 3b) which meant the light environment was highly diffuse and relatively stable. This led to very smooth light profiles and reasonable agreement between downcast and upcast for most stations (*see* Supplementary Fig. S7). The SSD003 downcasts were selected for further analysis, and we computed spectral diffuse attenuation coefficients (K_d) at each wavelength, for light data above and below the Secchi depth (Z_{SD}), by fitting a Beer–Lambert law to the light and depth data (*see* Supplementary Fig. S8). Additionally, we produced profiles of $K_d(z)$, where z = depth, by gridding the light profiles to a common depth grid (every 1 cm between surface and 15 cm above the maximum depth) and dividing the logarithmic difference between consecutive light measurements by the difference in depth. As the $K_d(z)$ profiles were noisy, they were smoothed using a Savitzky–Golay filter (with a kernel of 30 measurements and a

polynomial of one [linear], using Python function *scipy.signal. savgol_filter*), and seen to agree with K_d estimated above and below Z_{SD} from the Beer–Lambert law fits (*see* Supplementary Fig. S9).

We observed large differences in the magnitude and spectral shape of K_d in the Secchi depth layer over the course of the tidal cycle (Fig. 5a,b), with the magnitude decreasing at all wavelengths (Fig. 5a), and there being less attenuation for blue and green wavelengths, relative to red wavelengths, with increasing tide (Fig. 5b). We also found very good consistency between Z_{SD} data and K_d, represented by an exponential relationship (e.g., for 480 nm, *see* Fig. 5c, $r^2 = 0.73$, $p < 0.001$, and for min(K_d) [555 nm], $r^2 = 0.68$, $p < 0.001$), consistent with previous studies in estuaries, lakes, and coastal waters (e.g., Alikas and Kratzer 2017). The Secchi depth changed from approximately 1.5 m at low tide to over 4 m at high tide (Fig. 5c). Interestingly, we observed no such notable variations in the Forel Ule color (mean of 8.9, standard deviation of 2.2),
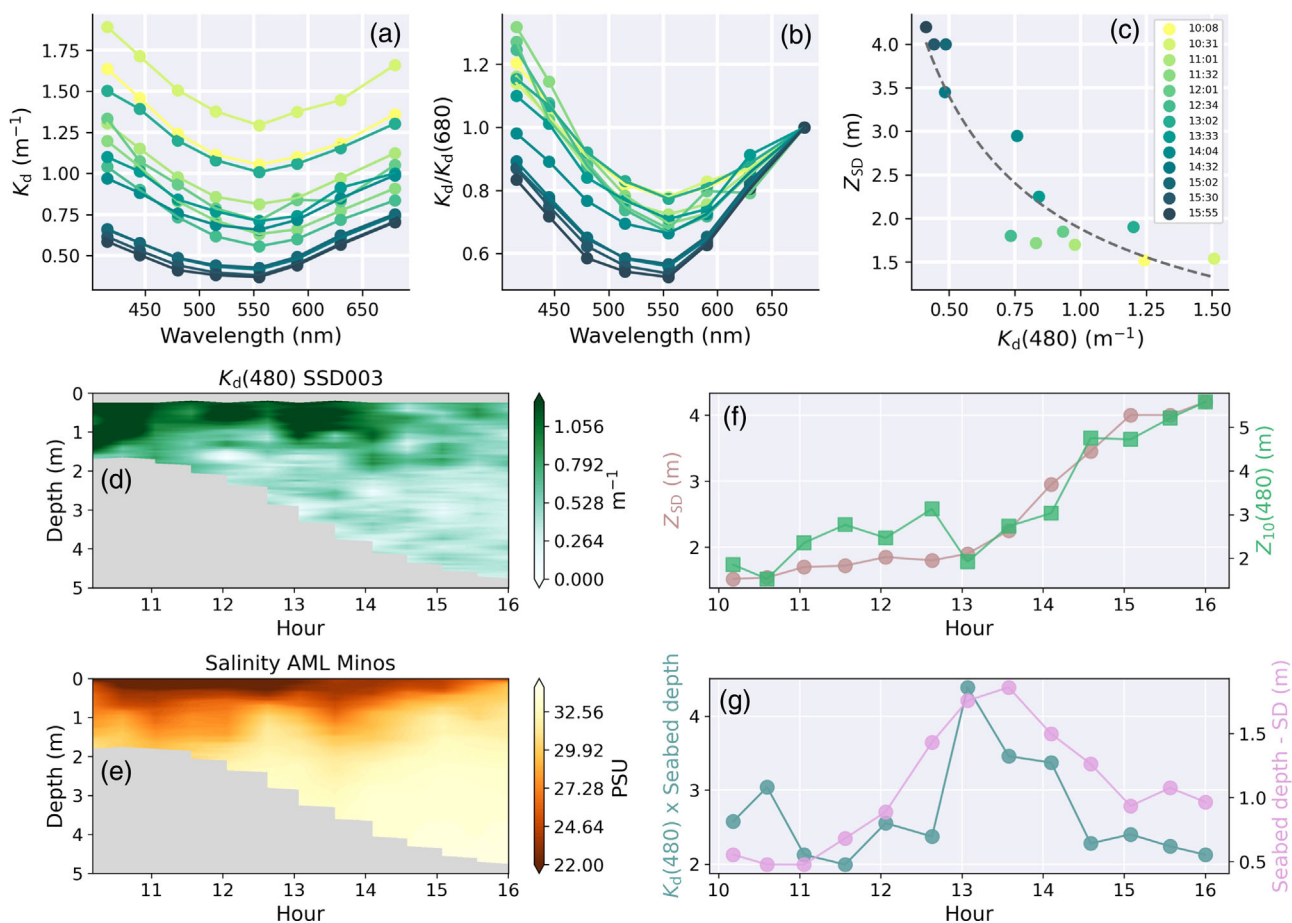

Fig. 5. Optical properties of the water derived using the SSD003 over a tidal cycle at Trelissick pontoon on 03 February 2023. (**a**) Spectral diffuse attenuation (K_d) for the 13 deployments over the tidal cycle in the Secchi depth layer. (**b**) Spectral variations in the shape of diffuse attenuation ($K_d/K_d(680)$) over the 13 deployments. (**c**) Relationship between the Secchi depth (Z_{SD}) and $K_d(480)$ for the 13 deployments. Gray dashed line shows an exponential fit to the data. (**d**) Contour plots of profiles of $K_d(480)$ derived using the SSD003. (**e**) Contour plots of profiles of salinity from the AML Minos. (**f**) Variations in Z_{SD} and the estimated 10% light level of 480 nm (2.3/$K_d(480)$) over the tidal cycle. (**g**) Relative light level at the seabed (seabed depth multiplied by $K_d(480)$), and the difference between the seabed depth and Z_{SD}, over the tidal cycle.

though the green color observed visually was consistent with the minimum K_d being at green wavelengths for all stations (555 nm, Fig. 5a). K_d above and below the Secchi depth layer was seen to be different for the first nine deployments, with systematically lower values below the Secchi depth layer (Supplementary Figs. S8, S9), suggesting clearer water at depth. Contour plots of $K_d(z)$ further illustrate these depth variations in K_d (Fig. 5d). When compared alongside the salinity data from the AML Minos CTD (Fig. 5e), the SSD003 data show how the freshwater in the estuary was considerably more turbid than the seawater and explains the large changes in Secchi depth observed over the tidal cycle, with the water at the Pontoon becoming diluted with clearer seawater as the tide pushes up (Fig. 5f). The Secchi depth was found to be in good agreement with the 10% light level at 480 nm ($2.3/K_d(480)$) in the Secchi layer (Fig. 5f), consistent with previous work (Lee et al. 2018b). Interestingly, when we multiply $K_d(480)$ by the depth of the seabed (extracted from the SSD003), we see that the relative light level at the seabed was lowest (i.e., less amount of surface light reaching the seabed) around mid-tide (Fig. 5g), which is further supported by the fact that the difference between the depth of the seabed and Secchi depth was highest at mid-tide. This may influence the photophysiology of organisms living at the seabed (i.e., they may be sensitive to the tidal cycle at the site). The analysis of data collected using

the SSD003 at Trelissick pontoon highlights its use for studying the optical environment of shallow estuaries, with the data collected showing good consistency with previous understanding (Alikas and Kratzer 2017; Lee et al. 2018b).

Loch Etive and Loch Creran, Oban, Scotland

We tested the SSD during two days of sampling at Loch Etive and Loch Creran (Oban, Scotland) on the 23 May 2023 and 25 May 2023, respectively (Fig. 6a), on the Scottish Association of Marine Science (SAMS) research vessel the RV *Seòl Mara* (Fig. 6b), for water depths ranging from 0 to 145 m. Data were collected at station RE05 at Loch Etive on 23 May 2023, and at stations LY0, LY1, LY2, LY4, CYLL, C1, C2, C3, C4, C5, and C6, at Loch Creran on 25 May 2023 (Fig. 6a). We note that station LY0, unlike all other stations, is not a standard station sampled by SAMS, but we named the station LY0 here just to reflect the fact it was seaward of LY1. The RV *Seòl Mara* operates an SBE 55 ECO Water Sampler and profiling frame that the vessel deploys using a winch on the aft deck (Fig. 6b). On the profiling frame (Fig. 6d), there are a number of additional sensing packages sampling at 1 Hz, including a SBE19 plusV2 SeaCAT (calibrated on 07 August 2007), measuring profiles of temperature and depth, and a Satlantic PAR sensor (calibrated on 14 January 2022), both of which were utilized in this study (Fig. 6d). At each station, the profiling frame was
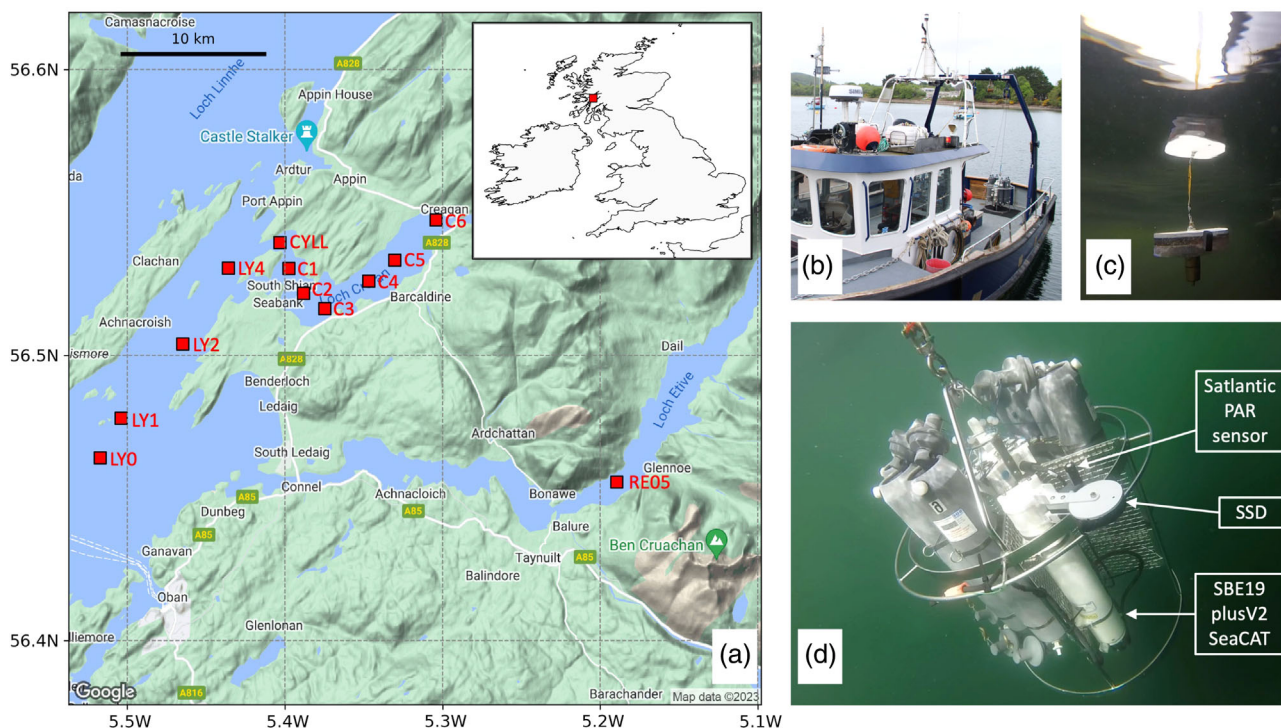

Fig. 6. (**a**) Location of stations sampled at Loch Etive and Loch Creran (red squares) near Oban, Scotland on 23 May 2023 and 25 May 2023 (background image is from Google Maps). (**b**) Photograph of research vessel (RV *Seòl Mara*) used for deploying equipment (note the CTD profiler on the aft deck winch). (**c**) Underwater shot (using Go-Pro) of an SSD (SSD002) deployed from a midi-Secchi disk in Loch Etive. (**d**) Underwater shot (using Go-Pro) of profiler deployed in Loch Creran, showing locations of Satlantic Photosynthetically Available Radiation (PAR) sensor, the SSD (SSD004) and the SBE19 plusV2 SEACAT CTD.

dipped into the surface water (1–2 m depth) and left to equili-brate for around 2 min, before profiling at around 16 cm per second, sampling the full water column. Only data collected on the profiling frame below 2 m depth were used in the comparison, to remove data while the instruments were equilibrat-ing, and avoid extreme cases of ship shadow or surface reflections from the metallic profiling frame.

Three SSDs were tested (SSD002, SSD003, and SSD004) dur-ing the sampling in Scotland. SSD004 (used at Loch Creran) and SSD003 (used at Loch Etive) were mounted to the SBE 55 ECO Water Sampler and profiling frame using the SSD pro-filing bracket (Fig. 1b) and placed near to both the SBE19 plusV2 SeaCAT and Satlantic PAR sensor (Fig. 6d). Only SSD data collected on the profiling frame below 2 m depth were used in subsequent comparisons to be consistent with the Sea-Bird and Satlantic sensor processing. The SSD002 was also deployed using a midi-Secchi disk (Fig. 6c), lowered to the sur-face, and left to equilibrate for 1–2 min before the profile com-menced. The SSD002 was lowered at a rate of around 17 cm per second (downcast) and retrieved (upcast) at around 25 cm per second on average. The SSD002 was deployed at both Loch Creran and Loch Etive, with the only station not sampled being C6. The SSD002 data from the midi-Secchi disk were processed in the same way as in the Trelissick pontoon deployments, by computing the cumulative sum of the gradient in the depth measurements and selecting a cut off value to remove data before and after the profile commenced (*see* Supplementary Fig. S4), and removing any data from the downcast that did not stay above the cut off value for more than 10 measurements. The only difference was that the cut-off value was increased to 0.4, following inspection of the data, owing to a faster sampling rate. Additionally, considering the device rarely approached the seabed, we kept all data around the maximum depth. The SBE19 plusV2 SeaCAT profiles were interpolated to the depth grid of the SSDs', for computing mean differences (δ) and mean absolute differences (Δ) in temperature.

For the comparison on the profiling frame, between the Satlantic PAR sensor and the light sensors on the SSD003 and SSD004, we fitted a Beer–Lambert law to the light and depth data for each sensor (both down and upcasts), to derive K_d for each profile, allowing a broad comparison of the depth gradi-ents in light attenuation between the two sensing packages. When comparing Satlantic PAR with the SSD, we used the clear channel on the SSD, which gives an approximation of integrated light over visible wavelengths, acknowledging that the spectral response function of the clear channel on the AS7341 is not a perfect representation of PAR (*see* fig. 1 of Bäumker et al. 2021). For the SSD002, we computed spectral K_d, for each of the eight wavebands, by fitting a Beer–Lambert law to the light and depth data of the profile (<20 m depth). Secchi depth data and Forel Ule data were collected with the SSD002 and other mini-Secchi disks, by participants on the research vessel, with median values and standard deviations computed at each station.

The sampling of Loch Creran on 25 May 2023 was aligned with a satellite overpass of the Sentinel 2B MultiSpec-tral Instrument (S2B), and we were fortunate to have relatively clear skies. Level 1C S2B data (S2B_MSI_2023_05_25_11_45_46_T30VUH_L2W.nc) were downloaded freely from the Sentinel Hub and processed using the open-source ACOLITE software (https://github.com/acolite/acolite). The image was atmospherically corrected (Vanhellemont 2020) using default ACOLITE settings to produce Level 2 above surface spectral reflectance at three visible bands (492, 559, and 665 nm), and the Secchi depth and spectral K_d for the three bands were esti-mated using the algorithm of Pitarch and Vanhellemont (2021), included in the ACOLITE software. Matchups between in situ data and S2B were extracted by selecting the nine pixels closest to the location of the in situ data point and com-puting median values and standard deviations.

The comparison of SSD temperature profiles with the SBE19 plusV2 SeaCAT are shown in Fig. 7. Station RE05 at Loch Etive is in deep water (~145 m) and has unique tempera-ture characteristics related to the physical dynamics of the Loch (*see* Edwards and Edelsten 1977). The SSD004 failed at around 70 m on the down cast, illustrating limitations in its design for sampling deeper into the water column. This was not intended originally and could potentially be addressed by modifying its design (*see* discussion). Fortunately, the SSD004 began working again afterwards, and we could extract the downcast which was found to be in excellent agreement with the SeaCAT (Fig. 7, $\delta = 0.00$ $\Delta = 0.1°C$). Consistent with the SSD004, the temperature profiles from the SSD003 at Loch Creran also compared very well with the SBE19 plusV2 Sea-CAT (Fig. 7). The comparisons indicate a mean difference of $-0.06°C$, and mean absolute difference of 0.04°C, which is well within the 0.1°C accuracy reported by the TMP117 manu-facturer. However, the mean difference was slightly more neg-ative on the upcast ($-0.1°C$) than the downcast ($-0.04°C$), possibility related to the slower response time of the TMP117 when compared with a commercial thermistor. We repeated the analysis using the SSD002 deployed on the midi-Secchi disk in the top 20 m (*see* Supplementary Fig. S10) which also showed very good agreement with the SeaCAT ($\delta = -0.02$, $\Delta = 0.08°C$), with no major differences in up and down casts. The results for the comparisons between SSD and SeaCAT agree with those using the AML Mino CTD (Fig. 4, $\delta = -0.04$, $\Delta = 0.02°C$), lending confidence in the performance of the SSD for measuring temperature profiles.

The comparison of SSD light profiles with the Satlantic PAR sensor are shown in Fig. 8 (*see* also Supplementary Fig. S11 for comparison with the SSD002 deployed on the midi-Secchi disk with Satlantic PAR on the profiling rig). As the SSD light data were uncalibrated, the scales of the two axes were aligned (by computing the mean differences and scaling the axes) to visually overlay the data and compare the gradients in light. Overall, the light gradients are in broad agreement, with the mean differences in K_d between the SSD and Satlantic PAR
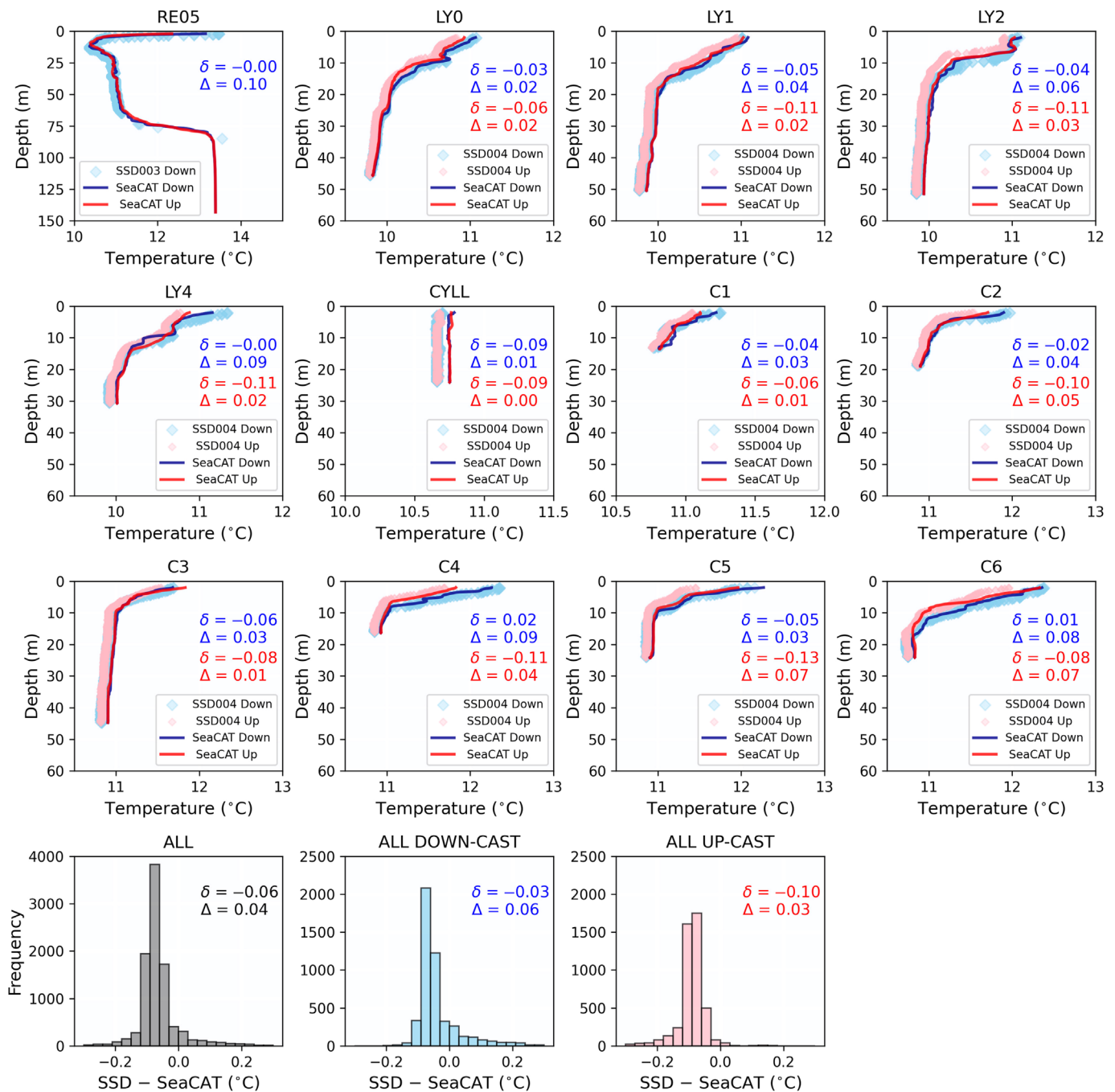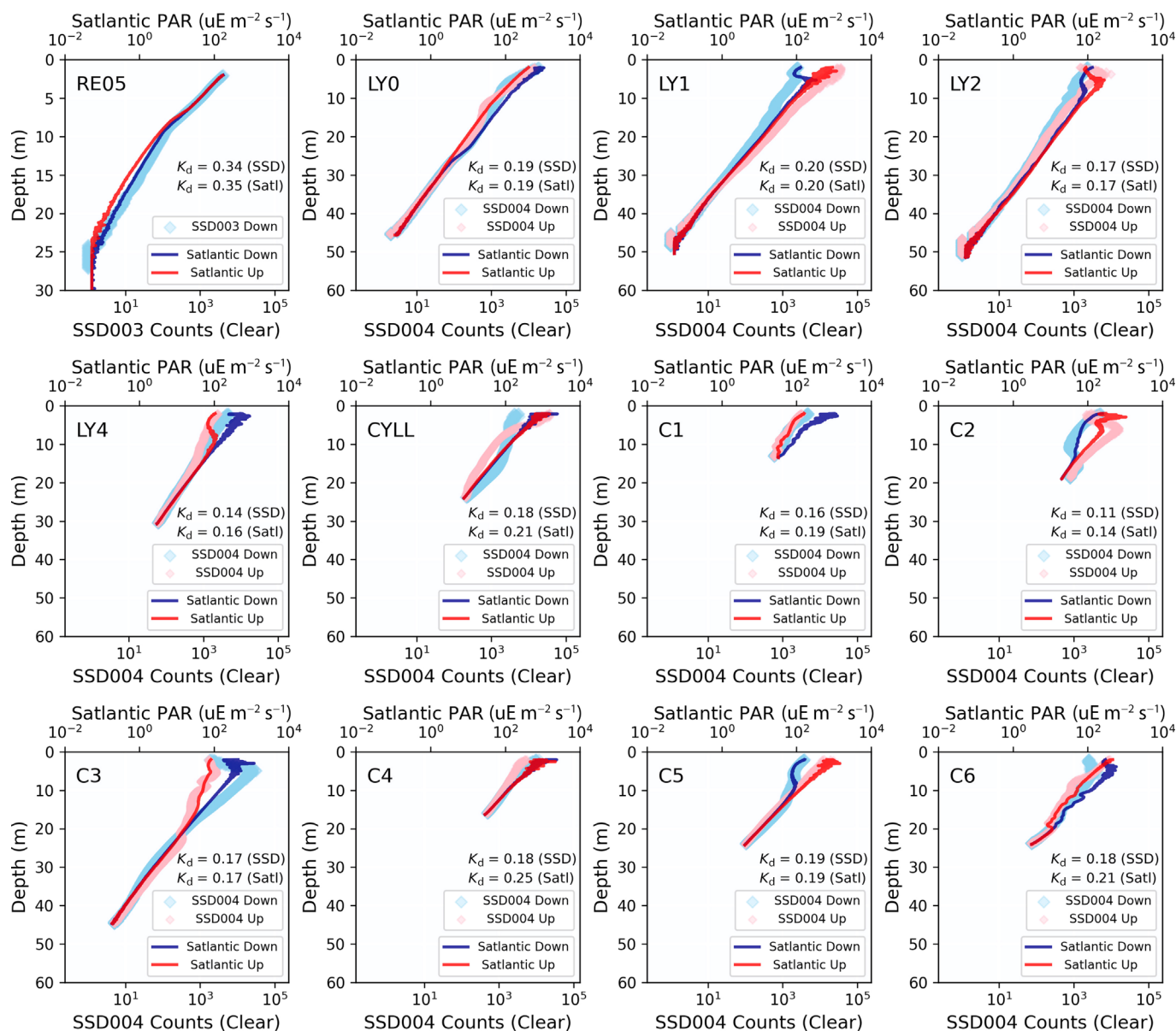
Fig. 7. Comparison of vertical temperature profiles collected during sampling at Loch Etive (RE05) and Loch Creran (LY0, LY1, LY2, LY4, CYLL, C1, C2, C3, C4, C5, C6) on 23 May 2023 and 25 May 2023, from a SBE19 plusV2 SeaCAT and a SSD mounted on a SBE 55 ECO Water Sampler (*see* Fig. 6d). δ represents the mean difference and Δ is the mean absolute deviation (red upcast, blue downcast, black all data).

being 0.02 m^{-1} and in good agreement ($\pm 0.01 \text{ m}^{-1}$) for 6 of the 12 stations (Fig. 8). At station RE05, the profiles of both sensors were very smooth, owing to very diffuse ambient light (23 May 2023 was a fully overcast day). Whereas, for the Loch Creran stations, there were some strange features in some of the profiles (Fig. 7), for both SSD and Satlantic PAR, likely due to the ambient light environment having a higher amount of

direct light (25 May 2023 had relatively clear skies), meaning the measurements were more susceptible to effects like shadow and reflections from the vessel and profiling frame. Nonetheless, many of these features were consistent between sensors.

Fig. 9 shows a map of the Sentinel 2B MSI (S2B) scene taken on 25 May 2023 with data collected using the

Fig. 8. Comparison of vertical profiles of light collected during sampling at Loch Etive (RE05) and Loch Creran (LY0, LY1, LY2, LY4, CYLL, C1, C2, C3, C4, C5, C6) on the 23 May 2023 and 25 May 2023, from a Satlantic (Satl) PAR sensor and a SSD mounted on a SBE 55 ECO Water Sampler. The SSD data are from the clear channel of the AS7341 sensor. Note the SSD light data are uncalibrated and the scales of the two *x*-axes have been aligned to visually compare the gradients in light from the two packages. The diffuse attenuation coefficient (K_d) is shown in black for each profile, for the two sensing packages.

SSD002 overlain, and Fig. 10 shows a more detailed comparison of each match-up. For all stations, except C6 (blocked by cloud), matchups were available. In general, the shape of the spectral diffuse attenuation coefficients ($K_d(\lambda)$) are in good agreement between S2B data and SSD data (Figs. 9b–d, 10), with lowest values at green wavelengths, followed by blue and red wavelengths. Across all stations, $K_d(665)$ is systematically higher than K_d for neighboring red bands derived by the SSD (Figs. 9d, 10). For matchups at stations within 1 h 15 min of the S2B over pass (Fig. 10, CYLL,

C1, C2, C3, C4, and C5), there is good agreement for K_d at blue and green wavebands (492 and 559 nm) between S2B and the SSD (though a small difference at C2), and excellent agreement close to the overpass (Fig. 10, C3). Interestingly, for the seaward stations, collected between 1.6 and 2.8 h prior to the SB2 overpass, K_d at blue and green wavebands (492 and 559 nm) for S2B are higher than the SSD (Fig. 10, LY0, LY1, LY2, LY4). All these stations were sampled within 1 h of high tide, whereas the S2B over pass occurred around mid-tide. Considering what we learnt from the sampling the Falmouth
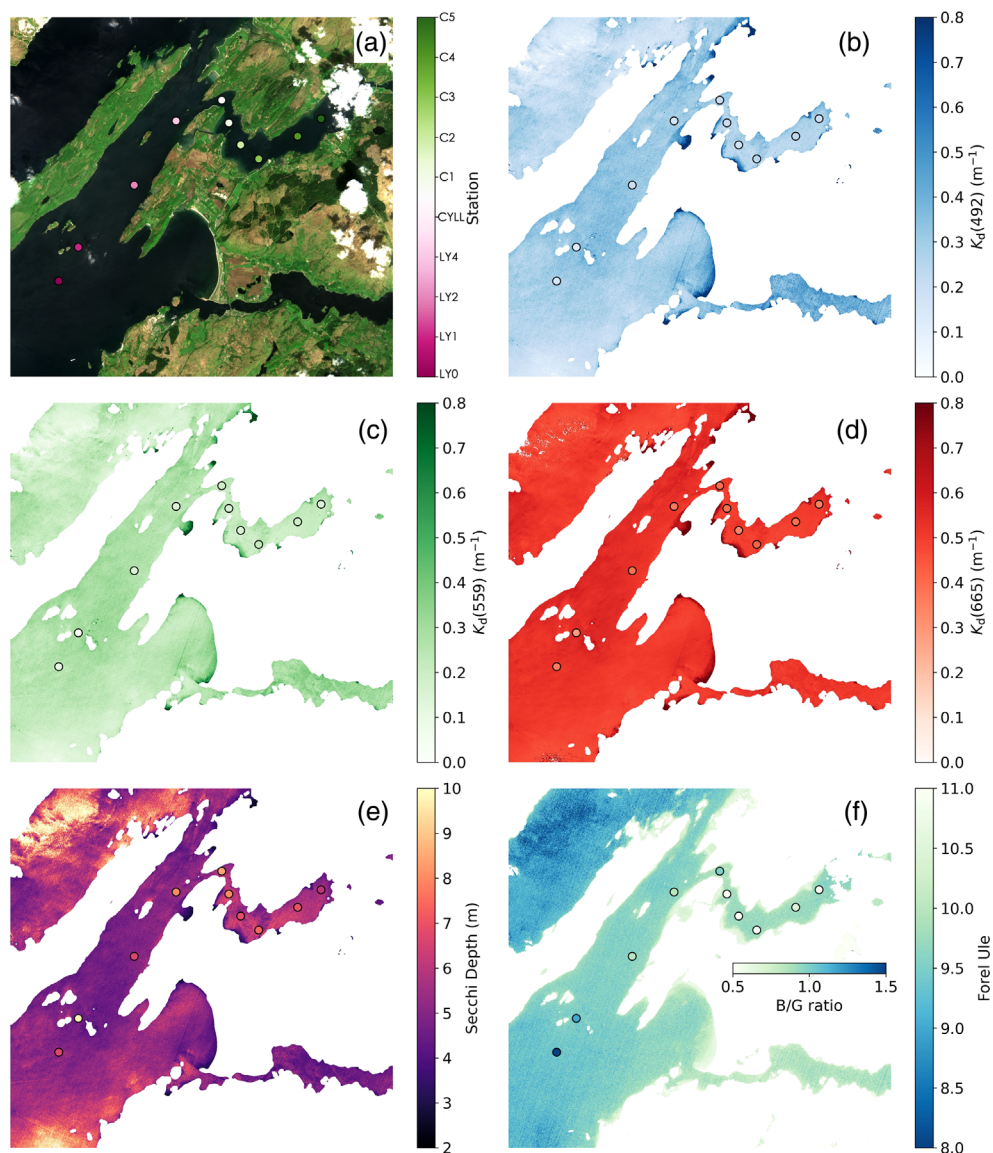
Fig. 9. Sentinel 2B MSI (S2B) scene taken on 25 May 2023 at 11:45 GMT and atmospherically corrected using ACOLITE software and processed using the in-water algorithm of Pitarch and Vanhellemont (2021). (**a**) True color image with the locations of the stations at Loch Creran sampled with the SSD on the mini-Secchi disk on the same day, overlain. (**b–d**) S2B diffuse attenuation coefficients (K_d) at 492, 559, and 665 nm respectively, with SSD in situ data overlain on the same color scale. The in situ data were spectrally interpolated (linear interpolation along the spectrum) from neighboring wavebands collected by the SSD, to match the wavebands of S2B. (**e**) Secchi depth maps with in situ data overlain (circles) on the same color scale. (**f**) Blue to Green reflectance ratio (B/G) of the satellite image, with in situ Forel-Ule data overlain.

estuary (Fig. 5), it is plausible that, as the tide dropped, more turbid water from the Loch moved seaward such that by the time S2B passed over, these stations had become more turbid. These results illustrate the requirement for a strict temporal matchup window between satellite and in situ data for estuarine regions with significant tidal ranges. Overall, S2B Secchi depth estimates were systematically lower than in situ data (Figs. 9e, 10, $\delta = -3.2$ m), but there was good agreement between the Forel Ule data and the ratio

of blue-green reflectance and K_d from S2B (Figs. 9f, 10), suggesting a greening of the water as sampling progressed up the Loch, seen with in situ and satellite data. SSD in situ K_d and Secchi depth data also agreed well, showing decreasing water clarity toward the source of the Loch. It is worth noting that satellite Secchi depth estimates depend on the accuracy of the input remote sensing reflectance data, in absolute and relative terms, whereas Forel-Ule color estimates depend on the relative weight of the remote sensing
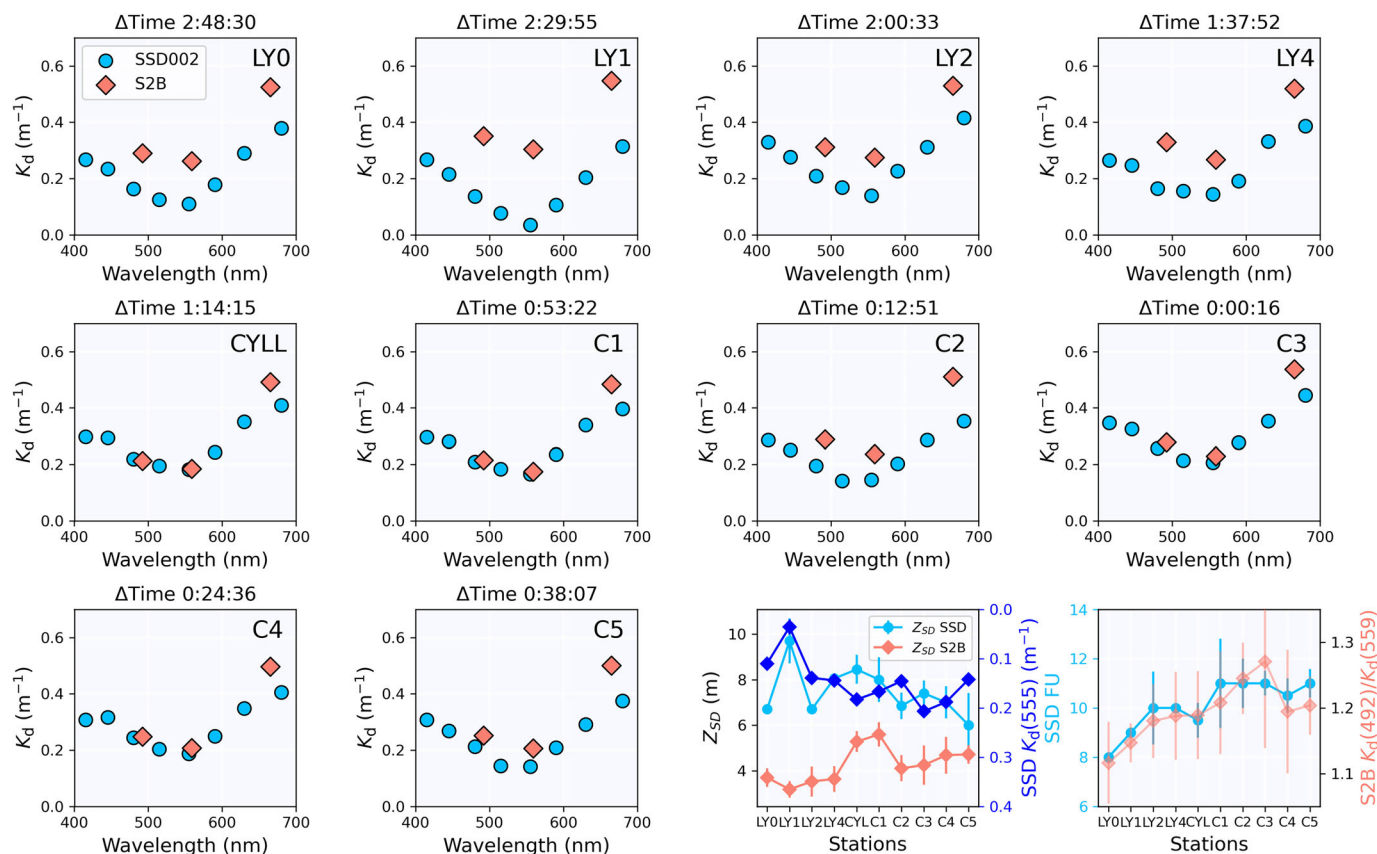
Fig. 10. Matchups at Loch Creran stations of optical data collected with the SSD (on the midi-Secchi disk) and that processed from the Sentinel 2B MSI (S2B) scene on 25 May 2023. Stations are denoted on the top right of the figures, with the title showing the time difference (HH : MM : SS) between the satellite overpass and the start of sampling at the station. The two figures on the right side of the bottom row show spatial variations in the Secchi depth (Z_{SD}) (both SSD and S2B) and Forel-Ule color (FU) between stations, with the SSD $K_d(555)$ and S2B $K_d(492)/K_d(559)$ ratio overlain, respectively, for the two plots.

reflectance bands, and so are likely to be less sensitive to atmospheric correction errors.

Discussion

Future improvements

Motivated by a need for an affordable optical sensing package that can be deployed from a variety of platforms, we have designed and built a low-cost SSD that combines historic and modern methods for monitoring the optical properties of water. Results from the assessments illustrate that the SSD, in addition to being used to measure the Secchi depth and Forel-Ule color, can collect temperature profiles within <0.1°C of commercial CTD instruments, and is capable of retrieving spectral diffuse attenuation coefficients at eight wavebands in the visible spectrum, with tests on the clear channel showing good consistency with a commercial PAR sensor (mean difference in K_d(PAR) of 0.02 m^{-1}). Nonetheless, despite meeting targets in design, performance, and cost, we acknowledge this is just a 1st prototype, and that improvements and further testing are required.

Questions remain on the durability and stability of the device and its performance over time, that will need to be addressed in future studies. For example, although protected by the 3D-printed base of the SSD, the putty used on the MS5803-14BA pressure sensor is fragile and may be prone to degradation. The prototype is set entirely in epoxy resin, to integrate the components into a small space, make the device water and pressure resistant, and to secure its circuitry. As highlighted in the assessment at Loch Etive, one of the devices failed at around 70 m depth, suggesting improvements are needed to make the device resistant to higher pressure. Improving the strength of the epoxy may help (e.g., using a different type of epoxy with stronger properties, or adding fiberglass to improve strength) or modifying the design of the device to strengthen the fixing of components exposed to the environment (e.g., where the pressure sensor and light sensors are attached). The disadvantage of using epoxy is that it becomes difficult (though not entirely impossible) to replace components on the device. This does raise questions about the life cycle and sustainability of the package, and there may be other ways of meeting requirements without having to use

epoxy resin (e.g., using oil, or redesigning the device using epoxy, but in such a way to make it easier to replace components) to improve the sustainability and longevity of the SSD. Nonetheless, if it does fail, the device is not useless, as it can still be used for measuring Secchi depth and Forel-Ule color. In fact, the heavy epoxy often means additional weight does not need to be added for the disk to sink vertically in the presence of low to moderate currents, unlike the standard mini-Secchi disk.

Although we have successfully managed to extract profiles from all deployments of the SSD wirelessly using the WiFi-connected webserver, at times it can be a frustrating process, and occasionally temperamental and slow. The original prototype used an MRK1000 and 5 V/1 A wireless charger. Subsequent iterations using an MRK1010 suggest a 5 V/5 A wireless charger works more efficiently with data transfer. Wireless data transfer could be sped up by compressing the data prior to transfer, or using other wireless methods, such as Bluetooth or cellular data transfer, that have had success in other projects (Bresnahan et al. 2022). These other wireless data transfer methods are also more suited to rapid data upload to servers, either through phone apps (Bluetooth) or directly by cellular data transfer. These methods have also been integrated into similar sized microcontrollers (e.g., Arduino MKR GSM 1400). Sever based uploads would also allow easy integration of data collected over wide areas, to study a broad range of optical environments, potentially increasing the number of end users and enhancing the impact of the data collected.

The spectral light sensor was found to operate well in a range of environments in the assessments, but certainly provided smoother light profiles in the presence of a diffuse (e.g., overcast skies) light environment. In direct light, it can struggle to cope with wave focusing, shadows (e.g., from clouds) and other surface reflections, like many light sensors. Near surface measurements and more sensitive to reflection effects. Near surface data collected at Trelissick pontoon and the Loch sites in Scotland may have been affected from light reflection from the pontoon and vessel. Correcting for such effects is not trivial and would require additional measurements to quantify and validate. It may be that improvements can be made to the designs of the SSD so that the light sensor can operate better in the presence of direct light, for example, by including a cosine corrector (not included in the 1st prototype as they can be fragile and costly) to improve hemispherical light detection, or to minimize surface reflection by measuring changes in upwelling rather than downwelling light (suggested following a personal communication with Dr ZhongPing Lee). However, such improvements would need to balance the need to keep the device low cost and relatively robust (e.g., for participatory science projects).

One potential issue with the design of the light sensor on the SSD, is that it is placed on a white reflective disk (or near to one, if the developer chose to use a checkered black and white Secchi disk and placed it in the black checkered part). In sediment laden turbid environments, with particles scattering light in multiple directions, the white disk will reflect light backwards that could be re-scattered by particles back into the sensor. There may also be issues with reflection of the white disk at the surface impacting the light data near to the very surface (*see* Fig. 6c for an example of this reflection). These issues may just require a simple correction to the processing, or other solutions could be explored, for example, having a detachable Secchi disk sitting on a black SSD that could be removed when profiling. Though not conducted here, the SSD light sensor could be calibrated to measure irradiance directly, extending its use for scientific applications, for example, as a simple tool to measure artificial night light in coastal waters, known to be a pressing environmental concern (Davies et al. 2014). The light sensor could also be adapted to measure PAR more accurately (*see* Bäumker et al. 2021). Future improvements in the light sensor should also take advantage of developments in sensing technology. For example, a new 14-channel light sensor (AS7343) has recently been released that could be integrated into future versions of the SSD, and could prove helpful for validating hyperspectral satellite ocean color missions like NASA's Plankton, Aerosol, Cloud, ocean Ecosystem mission (Werdell et al. 2019) and the Environmental Mapping and Analysis Program, as well as extracting more information on the compositions of particles and substances in the water. The spectral nature of the diffuse attenuation measurements may make it feasible to extract information on phytoplankton pigments and composition.

The temperature sensor (TMP117) performed very well in the comparisons with commercial CTDs. However, the response time of the TMP117 is never going to be as quick as a commercial CTD thermistor. This does limit the required profiling speed of the SSD needed to collect an accurate temperature profile, which is fine for present applications (e.g., shallow water surface profiling). However, if a faster profiling speed is needed, future developments in the SSD could look to integrate other temperature sensors with a faster response, like those used on a commercial CTD, but decisions would need to consider costs and impacts on sensor stability. In addition to improving existing sensing technology (light, pressure, and temperature sensing), there is scope to attach other sensors to the SSD. Having conductivity would be useful for measuring salinity, and together with temperature, could help improve depth measurements from the pressure transducer by correcting for density. Fluorescence (for chlorophyll *a*, dissolved organic matter, phycocyanin and phycoerythrin), backscattering and pH-based sensors could open the door to many other applications. The choice to integrate such sensor technology would need to consider requirements to keep the device small and low cost and whether achievable levels of sensor accuracy and stability would align with the needs of applications.

Should future SSDs be used widely, it would be worth developing simple tests that users could implement to increase

confidence in good fidelity sensing and to monitor calibration. For example, should a user want to measure absolute irradiance, dark counts could easily be measured and tracked using black electronic tape in a sink or bathtub. Similarly, temperature calibrations (at least to a course level) could be tracked using an ice bath, and pressure measurements using independent data on atmospheric pressure. Developing DIY calibration techniques could help overcome the need to send instruments off for regular calibration. A process that can be costly and take time, especially if it requires overseas shipping.

New insight and applications

Through developing a small (hand-held), low-cost optical sensing package, there is potential to expand optical profiling in lake, estuary, and shallow coastal waters, particularly in under-resourced regions, where monitoring organizations have not been able to afford commercial optical sensing packages. This could lead to new insight into the optical dynamics of regions not studied before. As the SSD offers a low-cost tool for evaluating satellite ocean and lake color (Figs. 9, 10), it may also be useful for identifying regional biases in satellite data and developing regional satellite algorithms, maximizing use of satellite imagery for environmental monitoring in understudied regions.

As the device is compact, it can be deployed from a wider variety of platforms, and consequently, expand the range of environments amenable to optical profiling. For example, we have successfully used it for vertical profiling in turbid tributaries of the Helford River in Cornwall, UK, from a kayak. This could lead to new insight into the optical dynamics of important, and hard to access, aquatic systems, such as around seagrass beds and coral reefs. The ergonomic design of the SSD and its low-cost manufacturing process makes the device particularly suitable for participatory (citizen) science projects, putting aquatic optical (and physical) profiling into the hands of anyone interested in helping to monitor the environment.

Combined use of the light and temperature profiling in the upper water column may offer insight into controls on the thermal structure of the surface layer and its relationship with water constituents that absorb light (e.g., biophysical coupling, *see* Sathyendranath et al. 1991). Additionally, water emissivity, a critical variable required for accurate satellite sea surface temperature (SST) estimates, is known to be related to turbidity (Wei et al. 2017). Spectral diffuse attenuation provides more information on the composition of substances in the water than turbidity alone and may offer insight into the relationship between ocean color and water emissivity, potentially improving satellite SST retrievals in coastal waters. This could be timely considering the developments in high spatial resolution thermal satellites (e.g., the CNES/ISRO Thermal infraRed Imaging Satellite for High-resolution Natural resource Assessment, the NASA and the Agenzia Spaziale Italiana Surface Biology and Geology

Thermal Infrared and the ESA/EU Land Surface Temperature Monitoring mission).

Secchi disker madness?

While acknowledging that, for a single profile with good quality measurements of K_d a Secchi disk may not be required "except perhaps for sentimental reasons" (Preisendorfer 1986, p. 39), there are other reasons why it may be useful to collect simultaneous measurements of Secchi depth (Z_{SD}) and K_d. Over the past decade there has been a resurgence in studying Secchi depth theory (*see* Lee et al. 2015, 2018b). Testing, developing, and studying new and historical theories around the Secchi depth require simultaneous measurements of Z_{SD} and K_d. Whereas the SSD is a low-cost optical profiling package, it will never be as cheap as a Secchi disk by its own right. If we take a situation of a participatory science project in a lake where Secchi disks were provided to citizens for monitoring lake clarity, it may be pertinent to include a few SSD-like instruments, to develop lake-specific relationships between Z_{SD} and K_d that could be used to convert the more numerous Z_{SD} data collected by the citizens into K_d data. Alternatively, converting K_d to Z_{SD} data could be useful when a user may want to approximate Secchi depth in waters shallower than this depth, where the measurement cannot be taken but a light profile can, although this would require a complex correction for contamination by light reflected from the bottom. We could also have a situation where long time-series data of Z_{SD} have been collected for many years, and the monitoring agency may want to maintain this time-series but begin measuring K_d directly. Finally, while the SSD is designed to measure light profiles and Secchi depth, it also provides useful and independent information on the thermal structure of the water column, all embedded into a single open-source sensing package.

Comments and recommendations

Spurred on by a need to develop low-cost optical sensing packages, due to the high cost of commercial optical sensors, we have demonstrated that it is possible to build an optical profiling package with respectable sensor accuracy and precision when compared with commercial sensors. The optical profiling package was integrated into an existing (and updated) hand-held tool (mini- and midi-Secchi disk), for measuring Secchi depth and Forel Ule color, combining historic and modern methods to monitoring optical properties of aquatic waters. The package has potential for low-cost monitoring, expanding observations in under-resourced regions, studying optical theory, validation of satellite remotely sensed data, for participatory science, and for communicating and teaching. Our approach to designing, developing, and manufacturing these tools has been to share our developments openly and

transparently with the community. We hope this will help fuel further innovation and benefit environmental monitoring.

References

Alikas, K., and S. Kratzer. 2017. Improved retrieval of Secchi depth for optically-complex waters using remote sensing data. Ecol. Indic. **77**: 218–227. doi:10.1016/j.ecolind.2017.02.007

Bardaji, R., A.-M. Sánchez, C. Simon, M. R. Wernand, and J. Piera. 2016. Estimating the underwater diffuse attenuation coefficient with a low-cost instrument: The KdUINO DIY buoy. Sensors **16**: 373. doi:10.3390/s16030373

Bäumker, E., D. Zimmermann, S. Schierle, and P. Woias. 2021. A novel approach to obtain PAR with a multi-channel spectral microsensor, suitable for sensor node integration. Sensors **21**: 3390. doi:10.3390/s21103390

Boyce, D. G., M. R. Lewis, and B. Worm. 2010. Global phytoplankton decline over the past century. Nature **466**: 591–596. doi:10.1038/nature09268

Bresnahan, P., and others. 2022. A high-tech, low-cost, internet of things surfboard fin for coastal citizen science, outreach, and education. Cont. Shelf Res. **242**: 104748. doi:10.1016/j.csr.2022.104748

Bresnahan, P. J., and others. 2023. Water quality monitoring and remote sensing validation with novel, technology-enabled citizen science devices. Poster session at the ASLO Aquatic Sciences Meeting.

Brewin, R. J. W., and others. 2017. Expanding aquatic observations through recreation. Front. Mar. Sci. **4**: 351. doi:10.3389/fmars.2017.00351

Brewin, R. J. W., T. G. Brewin, J. Phillips, S. Rose, A. Abdulaziz, W. Wimmer, S. Sathyendranath, and T. Platt. 2019. A printable device for measuring clarity and colour in lake and nearshore waters. Sensors **19**: 936. doi:10.3390/s19040936

Burggraaff, O., N. Schmidt, J. Zamorano, K. Pauly, S. Pascual, C. Tapia, E. Spyrakos, and F. Snik. 2019. Standardized spectral and radiometric calibration of consumer cameras. Opt. Express **27**: 19075–19101. doi:10.1364/OE.27.019075

Burggraaff, O., S. Panchagnula, and F. Snik. 2021. Citizen science with colour blindness: A case study on the Forel-Ule scale. PLoS One **16**: e0249755. doi:10.1371/journal.pone.0249755

Burggraaff, O., M. Werther, E. S. Boss, S. G. H. Simis, and F. Snik. 2022. Accuracy and reproducibility of above-water radiometry with calibrated smartphone cameras using RAW data. Front. Remote Sens. **3**: 940096. doi:10.3389/frsen.2022.940096

Busch, J. A., and others. 2016. Citizen bio-optical observations from coast- and ocean and their compatibility with ocean colour satellite measurements. Remote Sens. **8**: 879. doi:10.3390/rs8110879

Butler, J., and C. M. L. S. Pagniello. 2021. Emerging, low-cost ocean observing technologies to democratize access to the ocean. Oceanography **34**: 94–95. doi:10.5670/oceanog.2021.supplement.02-35

Chai, F., and others. 2020. Monitoring ocean biogeochemistry with autonomous platforms. Nat. Rev. Earth Environ. **1**: 315–326. doi:10.1038/s43017-020-0053-y

Davies, T. W., J. P. Duffy, J. Bennie, and K. J. Gaston. 2014. The nature, extent, and ecological implications of marine light pollution. Front. Ecol. Environ. **12**: 347–355. doi:10.1890/130281

Droujko, J., and P. Molnar. 2022. Open-source, low-cost, in-situ turbidity sensor for river network monitoring. Sci. Rep. **12**: 10341. doi:10.1038/s41598-022-14228-4

Edwards, A., and D. J. Edelsten. 1977. Deep water renewal of Loch Etive: A three basin Scottish fjord. Estuar. Coast. Mar. Sci. **5**: 575–595. doi:10.1016/0302-3524(77)90085-8

Eidam, E. F., T. Langhorst, E. B. Goldstein, and M. McLean. 2022. OpenOBS: Open-source, low-cost optical backscatter sensors for water quality and sediment-transport research. Limnol. Oceanogr. Methods **20**: 46–59. doi:10.1002/lom3.10469

Forel, F. A. 1890. Une nouvelle forme de la gamme de couleur pour l'étude de l'eau Des Lacs. Arch. Sci. Phys. Nat. Soc. Phys. Hist. Nat. Geneve **6**: 25.

Friedrichs, A., J. A. Busch, H. J. der Woerd, and O. Zielinski. 2017. SmartFluo: A method and affordable adapter to measure chlorophyll a fluorescence with smartphones. Sensors **17**: 678. doi:10.3390/s17040678

George, G., and others. 2021. Citizen scientists contribute to real-time monitoring of lake water quality using 3D printed mini Secchi disks. Front. Water **3**: 662142. doi:10.3389/frwa.2021.662142

Gillett, D., and A. Marchiori. 2019. A low-cost continuous turbidity monitor. Sensors **19**: 3039. doi:10.3390/s19143039

Griffiths, A. G. F., J. K. Garrett, J. P. Duffy, K. Matthews, F. G. Visi, C. Eatock, M. Robinson, and D. J. Griffiths. 2021. New water and air pollution sensors added to the sonic kayak citizen science system for low cost environmental mapping. J. Open Hardw. **5**: 1–18. doi:10.5334/joh.35

Groom, S., and others. 2019. Satellite ocean colour: Current status and future perspective. Front. Mar. Sci. **6**: 485. doi:10.3389/fmars.2019.00485

Harcourt, R., and others. 2019. Animal-borne telemetry: An integral component of the ocean observing toolkit. Front. Mar. Sci. **6**: 326. doi:10.3389/fmars.2019.00326

Hixson, J. L., and A. S. Ward. 2022. Hardware selection and performance of low-cost fluorometers. Sensors **22**: 2319. doi:10.3390/s22062319

Hommersom, A., and others. 2012. Intercomparison in the field between the new WISP-3 and other radiometers (TriOS Ramses, ASD FieldSpec, and TACCS). J. Appl. Remote Sens. **6**: 063615. doi:10.1117/1.JRS.6.063615

IOCCG. 2000. *In* S. Sathyendranath [ed.], Remote sensing of ocean colour in coastal, and other optically-complex, waters. Reports of the International Ocean-Colour

Coordinating Group, No. 3, IOCCG, Dartmouth, Canada. doi:10.25607/OBP-95

Kahru, M., Z. Lee, and M. D. Ohman. 2023. Multidecadal changes in ocean transparency: Decrease in a coastal upwelling region and increase offshore. Limnol. Oceanogr. **68**: 1546–1556. doi:10.1002/lno.12365

Kirby, R. R., G. Beaugrand, L. Kleparski, S. Goodall, and S. Lavender. 2021. Citizens and scientists collect comparable oceanographic data: Measurements of ocean transparency from the Secchi disk study and science programmes. Sci. Rep. **11**: 15499. doi:10.1038/s41598-021-95029-z

Kulk, G., G. George, A. Abdulaziz, N. Menon, V. Theenathayalan, C. Jayaram, R. J. W. Brewin, and S. Sathyendranath. 2021. Effect of reduced anthropogenic activities on water quality in lake Vembanad, India. Remote Sens. **13**: 1631. doi:10.3390/rs13091631

Lee, Z., S. Shang, C. Hu, K. Du, A. Weidemann, W. Hou, J. Lin, and G. Lin. 2015. Secchi disk depth: A new theory and mechanistic model for underwater visibility. Remote Sens. Environ. **169**: 139–149. doi:10.1016/j.rse.2015.08.002

Lee, Z., and others. 2018*a*. Global water clarity: Continuing a century-long monitoring. Eos **99**. doi:10.1029/2018EO097251

Lee, Z., S. Shang, K. Du, and J. Wei. 2018*b*. Resolving the long-standing puzzles about the observed Secchi depth relationships. Limnol. Oceanogr. **63**: 2321–2336. doi:10.1002/lno.10940

Leeuw, T., E. S. Boss, and D. L. Wright. 2013. In situ measurements of phytoplankton fluorescence using low cost electronics. Sensors **13**: 7872–7883. doi:10.3390/s130607872

Leeuw, T., and E. Boss. 2018. The HydroColor app: Above water measurements of remote sensing reflectance and turbidity using a smartphone camera. Sensors **18**: 256. doi:10.3390/s18010256

Malthus, T. J., R. Ohmsen, and H. J. van der Woerd. 2020. An evaluation of citizen science smartphone apps for inland water quality assessment. Remote Sens. **12**: 1578. doi:10.3390/rs12101578

Menon, N., G. George, R. Ranith, V. Sajin, S. Murali, A. Abdulaziz, R. J. W. Brewin, and S. Sathyendranath. 2021. Citizen science tools reveal changes in estuarine water quality following demolition of buildings. Remote Sens. **13**: 1683. doi:10.3390/rs13091683

Novoa, S., M. Wernand, and H. van der Woerd. 2014. The modern Forel-Ule scale: A "do-it-yourself" colour comparator for water monitoring. J. Eur. Opt. Soc. Rapid Publ. **9**: 14025. doi:10.2971/jeos.2014.14025

Novoa, S., M. Wernand, and H. J. van der Woerd. 2015. WACODI: A generic algorithm to derive the intrinsic color of natural waters from digital images. Limnol. Oceanogr. Methods **13**: 697–711. doi:10.1002/lom3.10059

Parra, L., J. Rocher, J. Escrivá, and J. Lloret. 2018. Design and development of low cost smart turbidity sensor for water

quality monitoring in fish farms. Aquacult. Eng. **81**: 10–18. doi:10.1016/j.aquaeng.2018.01.004

Pinsky, M. L., and A. Fredston. 2022. A stark future for ocean life. Science **1979**: 452–453. doi:10.1126/science.abo4259

Pitarch, J., and Q. Vanhellemont. 2021. The QAA-RGB: A universal three-band absorption and backscattering retrieval algorithm for high resolution satellite sensors. Development and implementation in ACOLITE. Remote Sens. Environ. **265**: 112667. doi:10.1016/j.rse.2021.112667

Preisendorfer, R. W. 1986. Eyeball optics of natural waters: Secchi disk science. NOAA Technical Memorandum ERL PMEL-67.

Rocher, J., J. M. Jimenez, J. Tomas, and J. Lloret. 2023. Low-cost turbidity sensor to determine eutrophication in water bodies. Sensors **23**: 3913. doi:10.3390/s23083913

Rodero, C., R. Bardaji, E. Olmedo, and J. Piera. 2022. Operational monitoring of water quality with a do-it-yourself modular instrument. Front. Mar. Sci. **9**: 1004159. doi:10.3389/fmars.2022.1004159

Sathyendranath, S., A. D. Gouveia, S. R. Shetye, P. Ravindran, and T. Platt. 1991. Biological control of surface temperature in the Arabian Sea. Nature **349**: 54–56. doi:10.1038/349054a0

Seafarers, S. D., S. Lavender, G. Beaugrand, N. Outram, N. Barlow, D. Crotty, J. Evans, and R. Kirby. 2017. Seafarer citizen scientist ocean transparency data as a resource for phytoplankton and climate research. PLoS One **12**: e0186092. doi:10.1371/journal.pone.0186092

Secchi, P. A. 1864. Relazione delle esperienze fatte a bordo della pontificia pirocorvetta l'Immacolata concezione per determinare la trasparenza del mare; Memoria del P. A. Secchi. Il Nuovo Cimento **20**: 205–238. doi:10.1007/BF02726911

Tyler, J. E. 1968. The Secchi disc. Limnol. Oceanogr. **13**: 1–6. doi:10.4319/lo.1968.13.1.0001

Ule, W. 1892. Die Bestimmung der Wasserfarbe in den Seen, p. 70–71. *In* Kleinere Mittheilungen. Dr. A. Petermanns Mittheilungen Aus Justus Perthes Geographischer Anstalt. Gotha, Justus Perthes.

Vanhellemont, Q. 2020. Sensitivity analysis of the dark spectrum fitting atmospheric correction for metre- and decametre-scale satellite imagery using autonomous hyperspectral radiometry. Opt. Express **28**: 29948–29965. doi:10.1364/OE.397456

von Schuckmann, K., and others. 2021. Copernicus marine service ocean state report, issue 5. J. Operat. Oceanogr. **14**: 1–185. doi:10.1080/1755876X.2021.1946240

Wang, Y., S. M. S. M. Rajib, C. Collins, and B. Grieve. 2018. Low-cost turbidity sensor for low-power wireless monitoring of fresh-water courses. IEEE Sens. J. **18**: 4689–4696. doi:10.1109/JSEN.2018.2826778

Wei, J.-A., D. Wang, F. Gong, X. He, and Y. Bai. 2017. The influence of increasing water turbidity on sea surface

emissivity. IEEE Trans. Geosci. Remote Sens. **55**: 3501–3515. doi:10.1109/TGRS.2017.2675623

Werdell, P. J., and others. 2019. The plankton, aerosol, cloud, ocean ecosystem Mission: Status, science, advances. Bull. Am. Meteorol. Soc. **100**: 1775–1794. doi:10.1175/BAMS-D-18-0056.1

Wernand, M. R. 2010. On the history of the Secchi disc. J. Eur. Opt. Soc. Rapid Publ. **5**: 10013s. doi:10.2971/jeos.2010.10013s

Wernand, M. R., and H. J. van der Woerd. 2010. Spectral analysis of the Forel-Ule ocean colour comparator scale. J. Eur. Opt. Soc. Rapid Publ. **5**: 10014s. doi:10.2971/jeos.2010.10014s

Wernand, M. R., H. J. van der Woerd, and W. W. C. Gieskes. 2013. Trends in ocean colour and chlorophyll concentration from 1889 to 2000, worldwide. PLoS One **8**: e63766. doi:10.1371/journal.pone.0063766

Ye, M., and Y. Sun. 2022. Review of the Forel–Ule Index based on in situ and remote sensing methods and application in water quality assessment. Environ. Sci. Pollut. Res. **29**: 13024–13041. doi:10.1007/s11356-021-18083-0

Conflict of Interest

T.G. Brewin and R.J.W Brewin are managing directors of Brewtek Ltd that produces and sells the open-source (designs openly available for commercial use) mini- and midi-Secchi disk. The remaining authors have no conflicts of interest to declare.